Chemical Physics Letters 458 (2008) 138–142

Contents lists available at ScienceDirect

Chemical Physics Letters

journal homepage: www.elsevier.com/locate/cplett

Silica nanotubes decorated with internal periodic rings

Ruying Li [a], Yong Zhang [a], Xiaorong Zhou [b,*], Xueliang Sun [a,*]

[a] Department of Mechanical and Materials Engineering, University of Western Ontario, 1151 Richmond Street, London, Ont., Canada N6A 5B9
[b] School of Materials, University of Manchester, Manchester M60 1QD, UK

ARTICLE INFO

Article history:
Received 22 November 2007
In final form 17 April 2008
Available online 23 April 2008

ABSTRACT

Silica nanotubes decorated with internal periodic rings have been synthesized via a chemical vapor deposition process with the aid of sulfur. The amorphous nanotubes have an outer diameter of 400–600 nm and wall thickness of 50–60 nm with the internal periodic ring being spaced approximately 220 nm apart. Selective growth of nanotubes or nanocables is controlled via a designed evaporation process. Sulfur has been proved to play an important role in inducing a transition from nanowires to nanotubes. Featuring their periodic rings, these silica nanotubes may find potential applications in various optical, electronic and catalytic nanodevices.

1. Introduction

Following the discovery of carbon nanotubes, non-carbon inorganic nanotube synthesis starting with layered precursors has been experimentally realized and various inorganic layered nanotubes have been subsequently developed [1–3]. More recently, inorganic nanotubes derived from non-layered structure such as SiO_2 [4–10], Al_2O_3 [11], TiO_2 [12], Ga_2O_3 [13], GaN [14], CdSe [15], CdS [16] and ZnS [17] have received increasing attention owing to both their tunable physical properties and high surface area featuring with reactive surface sites. Among various non-layered nanotubes, silicon oxide nanotubes have exhibited multi-functional nature due to their wide structural flexibility, high thermal and chemical stability as well as fine biocompatibility, which make them suitable candidates for field effect transistors [18], nanothermometers [19], nanoreactors [20], gas sensors [21], bio-molecular delivery [22] and catalyst support [23] applications.

As is known, more interesting physical/chemical properties are expected with the addition of complicated structures to nanotubes. Recently, silicon nanotubes with regular dome-shaped interiors have been synthesized using silane as the silicon source [24]. However, the reports on silicon oxide nanotubes with well-defined complex structures still remain lack. Metal with low melting point [19] or various sulfides [25,26] have ever been employed as the templates to grow silica nanotubes via chemical vapor deposition. However, the solid core inside the nanotubes can not be easily removed probably due to either capillary action or high melting point of the involved sulfides. In addition, all low melting point pure metals, such as gallium [27] and tin [28], are not applicable for generating silica nanotubes.

In the present study, we have used tin and sulfur as raw materials to synthesize a new type of hollow silica nanotube array through a carefully designed evaporation process via chemical vapor deposition. Interestingly, the nanotubes exhibit regularly spaced ring structure embedded on the internal surface of the nanotube wall. The structure of the nanotubes obtained here is similar to the so-called bamboo-like nanostructures reported previously, which have exhibited distinct cathodoluminescence [29] and electrocatalytic activity [30]. This kind of composite structure may also have potential applications in constructing various nanoscale functional devices for optical grating, light emitters, selective catalysis and other applications.

2. Experimental

Silica nanotubes were synthesized using a vacuum-free hot wall chemical vapor deposition system with a quartz tube (0.75 in. inner diameter and 30 in. length) being mounted horizontally at the centre of the furnace. Inside the quartz tube, temperature and gas flow rate are controlled. Sulfur and tin powders, in a weight ratio of 1:10000/min depending on duration time at the target temperature, were placed at the centre of the tube and the upstream of gas flow, respectively. A silicon substrate was placed 1 cm in the downstream from tin powder. High purity argon gas (99.999% argon, supplied by Praxair Canada Inc.) was employed as carrier gas which passed through the tube at a rate of 400 sccm (standard cubic centimeters per minute). At the beginning of the synthesis process, the reaction chamber was purged with argon gas for 20 min before being heated from room temperature to 900 °C within 15 min. The reaction chamber was kept at 900 °C for 10 min for the growth of short nanotubes or 60 min for the

* Corresponding authors. Fax: +1 519 661 3020 (X. Sun); +44 161 200 4865 (X. Zhou).
E-mail addresses: xiaorong.zhou@manchester.ac.uk (X. Zhou), xsun@eng.uwo.ca (X. Sun).

0009-2614/$ - see front matter © 2008 Elsevier B.V. All rights reserved.
doi:10.1016/j.cplett.2008.04.080

growth of long nanotubes. Then, the temperature was rapidly decreased to 800 °C and kept for 40 min. The reaction chamber was finally cooled to room temperature by flowing argon gas. The synthesized products were examined initially by using a Hitachi S-4500 field emission scanning electron microscope (FESEM). Further characterization of the nanostructures was carried out using a JEOL 2010 FEG transmission electron microscope (TEM) equipped with energy dispersive X-ray (EDX) analysis facility. The structure of the nanostructures was determined by a Tecnai G^2 F30 high-resolution transmission electron microscope (HRTEM).

3. Results and discussion

Fig. 1 shows scanning electron micrographs of the nanotubes grown on a silicon substrate. For the growth time of 10 min, short nanotubes of about 1 μm length were obtained, as illustrated in Fig. 1a. Increased magnification micrographs of a single nanotube are displayed in the inset of Fig. 1a. The upper image shows the top view of the nanotube while the cross-sectional image in the lower image reveals a clear tubular profile and cone-like shape of the nanotube. The outer diameter of the nanotube is approximately 500 nm at the opening end of the nanotube. For the increased growth time of 60 min, high density long nanotubes were produced along with some small rods and particles, as shown in Fig. 1b. The length of the nanotubes is about 20 μm.

Further structural and compositional analyses were carried out by TEM, as shown in Fig. 2. The outer diameter and wall thickness of the nanotube are approximately 600 nm and 55 nm, respectively. Further, a ladder-like feature along the nanotube, with the same intervals of about 220 nm, is evident. Low magnification TEM observation reveals that the ladder-like structure is the typical morphology of the nanotubes. By tilting the nanotube in TEM, it was revealed that the ladder-like feature actually corresponds to periodic 'O' rings embedded on the internal surface of the nanotube wall. The width of each ring is approximately 35 nm. Selected area electron diffraction (SAED) pattern of the nanotube displays clearly amorphous diffusion rings (inset of Fig. 2a), indicating the amorphous nature of the nanotube.

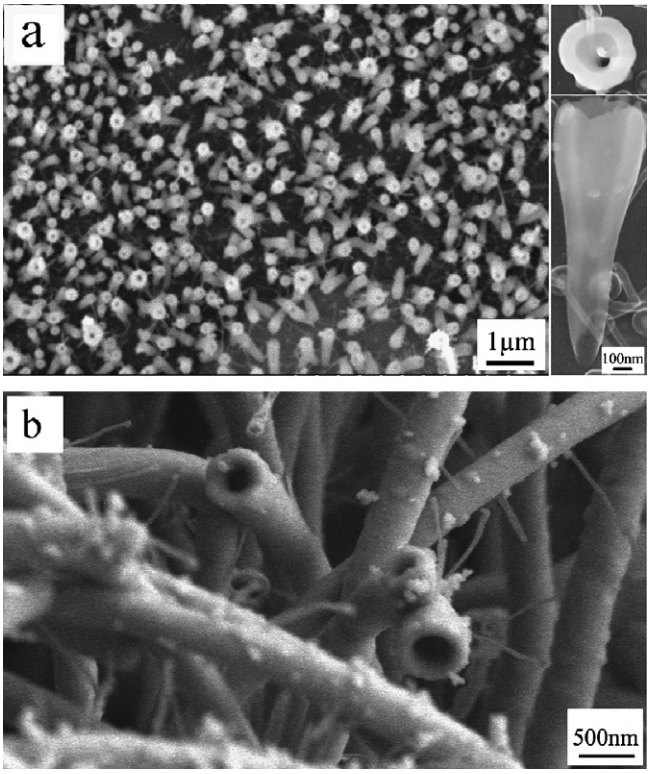

Fig. 1. Scanning electron micrographs of silica nanotubes grown on a silicon substrate with the growth time of: (a) 10 min; inset, top view (upper image) and cross-sectional view (lower image) of a single nanotube; and (b) 60 min.

EDX line scanning across the nanotube (as indicated by Line 1 in Fig. 2a) detected mainly silicon and oxygen with low yields of sulfur and tin (Fig. 2b). The X-ray intensity profiles for Si and O match the hollow nature of the nanotube very well. Fig. 2c–f display electron energy loss spectroscopy (EELS) maps of the nanotube con-

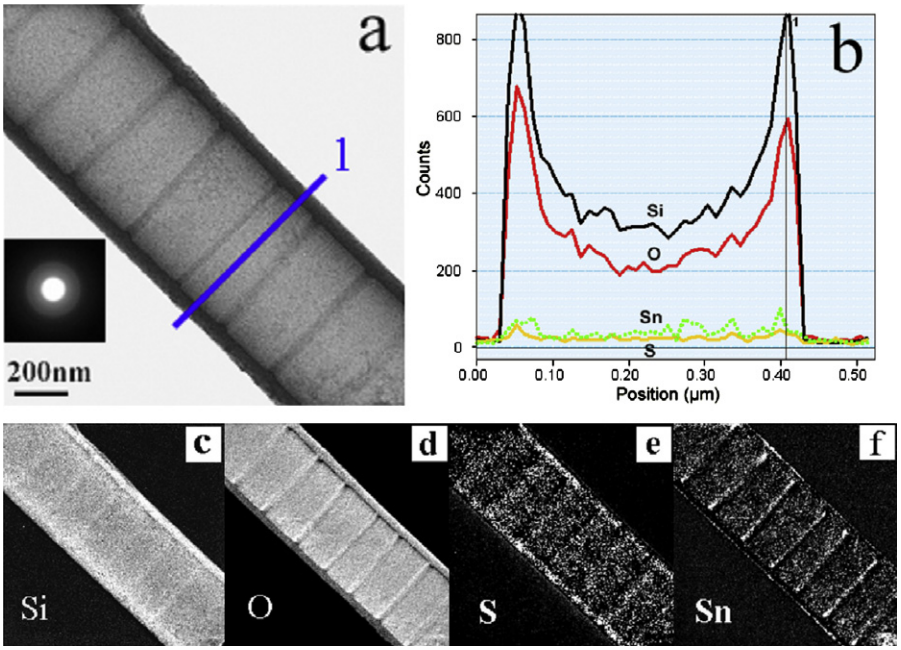

Fig. 2. (a) Transmission electron micrograph of the silica nanotube; (b) EDX line scanning profiles of the nanotube displayed in (a); and (c–f) EELS maps.

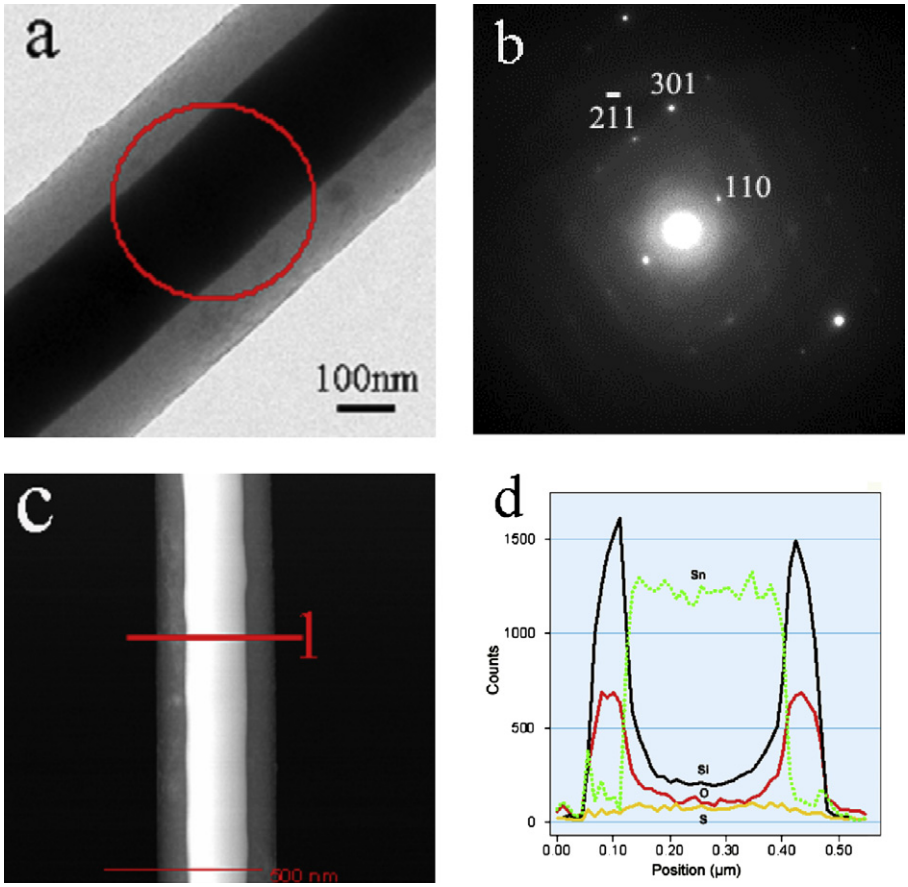

Fig. 3. (a) Transmission electron micrograph of the nanostructure formed under the same condition as that for the nanotube of Fig. 2, except for skipping the evaporation step at 800 °C; (b) diffraction pattern taken from the area indicated by the circle in (a); (c) HAADF image of the nanostructure; and (d) EDX line scanning profiles of the nanostructure displayed in (a).

firming the presence of Si, O, S and Sn species. As shown in Fig. 2e, sulfur element is uniformly distributed along the nanotube wall, which implies well incorporated sulfur within the silicon oxide nanotubes, while scrutiny of the tin map (Fig. 2f) revealed an increased level of tin on the outer surface of the nanotube wall and at the 'O' rings compared with the nanotube wall per se. Previous reports have displayed various advantages of sulfur doped silicon oxide, for example, lower optical losses [31]. The combination of sulfur doping and spaced ring structure in the silicon oxide nanotubes may bring them with potential applications, for example, optical gratings as exhibited in silicon oxide fibers [31].

In the present study, it has been found that hollow nanotubes or core/shell nanocables can be selectively synthesized with a carefully selected evaporation process. Considering tin's low melting point of 232 °C, for the growth of the nanotubes, an evaporation process at 800 °C for 40 min was employed after the reaction at 900 °C as mentioned in the experimental section. While the evaporation step at 800 °C was skipped, morphology, composition and structure details of the product are presented in Fig. 3. The bright field image of Fig. 3a clearly reveals a nanostructure consisting of a dark core and a bright shell. It is evident that the shell is featureless, suggesting amorphous nature. High angle annular dark field (HAADF) image of the nanostructure (Fig. 3c) exhibits a shell consisting of light elements and a core of relatively heavy elements. The diffraction pattern of the selected area (indicated by a circle in Fig. 3a) is displayed in Fig. 3b. The diffraction pattern can be indexed as metallic beta tin. EDX line scanning profiles across the nanostructure (as indicated by Line 1 in Fig. 3c) are illustrated in Fig. 3d. Compared with the EDX profiles of the nanotube shown in Fig. 2, it is clearly evident that the core of the nanostructure is metallic tin. Further, the Si, O and S profiles in Fig. 3c are consistent with those in Fig. 2b. Scrutiny of the tin profile revealed again an increased yield at the outer surface of the shell compared with the shell per se. Therefore, the results indicate that the tin/silica core/shell nanocables can be prepared by skipping the evaporation

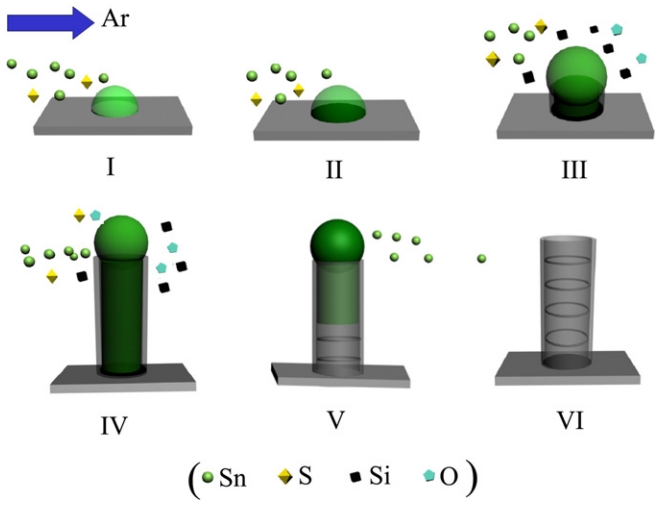

Fig. 4. Schematic diagram illustrating the growth mechanism of silica nanotubes decorated with internal periodic rings. (For interpretation of the references to colour in this figure legend, the reader is referred to the web version of this article.)

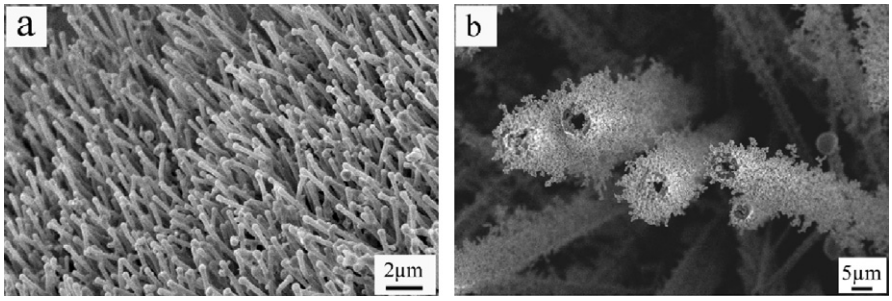

Fig. 5. Scanning electron micrographs of (a) silica nanowires while sulfur was not involved in the growth process; (b) silica nanotubes obtained from relatively high sulfur addition (S:Sn = 1:1000/min in weight ratio) in the starting material.

process. According to our SEM and TEM observations, almost 100% product was tin filled nanotubes without evaporation process. While the evaporation process was conducted, over 85% yield product was empty nanotubes with rings.

A two-step mechanism for the growth of silica nanotubes is suggested: first, a composite of silica nanotube/liquid tin core was synthesized on the silicon substrate at 900 °C using tin as the catalyst following the vapor–liquid–solid (VLS) process [27]. Second, liquid tin contained in the silica nanotubes was evaporated at 800 °C.

As illustrated schematically in Fig. 4, the growth process of silica nanotube with regularly spaced internal rings is proposed as follows:

When the temperature at reaction chamber reaches 900 °C, tin and sulfur vapors are generated by thermal evaporation from the molten tin and sulfur powder. The vapors are then transported downstream by the carrier gas (Ar) and then condense on the surface of silicon substrate located at the region of relatively low temperature in the form of liquid droplets. The liquid droplet provides an energetically favored site for the condensation of more incoming vapors, leading to the increase of the volume of liquid droplet (Fig. 4I). Then, at the silicon/tin liquid interface, liquid Sn–Si alloy is formed due to the relatively low melting point of the alloy (Fig. 4II) [32]. Subsequently, silicon vapor is generated from the liquid alloy by thermal evaporation. The alloying process between the liquid tin and silicon was confirmed by ex situ SEM examination of the silicon substrate, which revealed high density of pits on the substrate surface. The liquid alloy droplets continue to act as energetically favored sites for further condensation and absorption of Si, O, S and Sn species from the vapor phase. Oxygen is from the following three possible sources: (i) residual oxygen in argon gas [33]; (ii) the oxide layer on tin particles; and (iii) residual oxygen in the reaction chamber.

While the alloy droplet becomes supersaturated with the absorbed elements, we assume that two processes occur simultaneously here – one is the formation of silica nanotubes and the other is the growth of tin core.

For the growth of silica nanotubes, when the droplet becomes saturated with Si and O, the excess species form silica at the surface of the liquid droplet (Fig. 4III). Since the bond energy of Si–O is 799.6 kJ/mol, higher than that of Si–S (623 kJ/mol), Sn–O (531.8 kJ/mol) and Sn–S bond (464.0 kJ/mol) [34], silicon preferentially combines with oxygen to form stable silica. As far as tin liquid core growth is concerned, the lateral growth of the liquid tin core is efficiently suppressed by the formation of silica shell at the side surface. In this case, the liquid tin is encapsulated inside tubular silica. The coming tin species from vapor are absorbed on the top of the tin droplet to form one-dimensional liquid tin core in the silica nanotube. The continuous addition of Si, O, S and Sn species at top surface of the nanostructure consequently leads to the one-dimensional growth of silica shell/liquid tin core composite (Fig. 4IV).

When the temperature at reaction chamber decreases to 800 °C, the evaporation rate of liquid tin contained in the nanotubes exceeds that of absorption from the vapor phase because the tin's partial pressure decreases at 800 °C due to less evaporation from tin powder source when compared with that at 900 °C. The continuous evaporation of tin from the nanotubes leads to the retreating of the liquid/vapor interface inside the nanotube away from the substrate in order to maintain the surface area of the droplet on the top of the nanotube. The evaporation of tin also results in the aggregation of Si and O within the layer immediately near the liquid/vapor interface. The continuous aggregation of Si and O leads to the freezing out of a silica layer at the liquid/vapor interface because the solidification rate of glass is determined by its viscosity depending on temperature and composition [35]. The frozen silica layer of low viscosity is anchored to the wall of nanotubes when the evaporation of tin from the nanotubes continues and the surface of liquid tin continues to retreat. The anchoring and retreating introduce a tension to the frozen silica layer. When the tension within the layer reaches a critical level, the layer is disrupted and attached to the wall of the nanotubes to form a ring at the internal surface of the nanotube (Fig. 4V). And a new cycle of evaporation, solidification and disruption starts. The cyclic processes repeat until all liquid tin is evaporated (Fig. 4VI). Since the temperature was kept at 800 °C, the time needed for each cycle was approximately similar. Therefore, the 'O' rings are regularly spaced.

In our work, sulfur is shown to play a critical role in the formation of the tubular silica structure although it is still not very clear. As shown in Fig. 5a, when sulfur was absent from the reaction chamber, silica nanowires were obtained under the same synthesis conditions as that for the nanotubes. This is consistent with previous report on the synthesis of silica nanowires [28]. Further, when the weight ratio of sulfur to tin increased from 1:10000/min to 1:1000/min, as shown in Fig. 5b, nanotubes of increased diameter of about 1 μm, with high population density of sulfur particles being attached on the nanotube outer wall, were obtained. Further investigation is currently being undertaken to achieve a better understanding of the role of sulfur in the synthesis process.

4. Conclusions

In conclusion, an effective route to synthesize aligned and hollow silica nanotubes with distinct structure has been developed. The uniqueness of the resultant silica nanotubes is the regularly spaced periodic rings that decorate the internal surface of the nanotubes. The two-step growth mechanism suggests: (i) a composite of silica nanotubes/liquid tin nanowires is synthesized at 900 °C using tin as the catalyst; (ii) the nanotubes are generated by evaporation of tin from the composite; and (iii) the formation

of the periodic internal rings is the result of cyclic processes of evaporation of tin and solidification of silica at 800 °C. The novel silica nanotubes with periodic rings may find applications in optical, electronic and catalytic nanodevices.

Acknowledgments

This research was supported by Natural Sciences and Engineering Research Council of Canada (NSERC), Canada Research Chair (CRC) Program, Canada Foundation for Innovation (CFI), Ontario Innovation Trust (OIT), Ontario Early Researcher Award (ERA) and the University of Western Ontario.

References

[1] Y. Feldman, E. Wasserman, D.J. Srolovitz, R. Tenne, Science 26 (1995) 222.
[2] M.E. Spahr, P. Bitterli, R. Nesper, M. Müller, F. Krumeich, H.U. Nissen, Angew. Chem. Int. Ed. 37 (1998) 263.
[3] C.H. Ye, G.W. Meng, Z. Jiang, Y.H. Wang, G.Z. Wang, L.D. Zhang, J. Am. Chem. Soc. 124 (2002) 15180.
[4] H. Nakamura, Y. Matsui, J. Am. Chem. Soc. 117 (1995) 2651.
[5] J.B. Lee, S.C. Lee, S.M. Lee, H.J. Kim, Chem. Phys. Lett. 436 (2007) 162.
[6] E. Pouget et al., Nature Mater. 6 (2007) 434.
[7] X. Fan, X.M. Meng, X.H. Zhang, C.S. Lee, S.T. Lee, Appl. Phys. Lett. 90 (2007) 103114.
[8] C. Zollfrank, H. Scheel, P. Greil, Adv. Mater. 19 (2007) 984.
[9] X.W. Wu, J.F. Ruan, T. Ohsuna, O. Terasaki, S.N. Che, Chem. Mater. 19 (2007) 1577.
[10] D. Golberg, Y.B. Li, M. Mitome, Y. Bando, Chem. Phys. Lett. 409 (2005) 75.
[11] L. Pu, X.M. Bao, J.P. Zou, D. Feng, Angew. Chem. Int. Ed. 40 (2001) 1490.
[12] P. Hoyer, Langmuir 12 (1996) 1411.
[13] B. Cheng, E.T. Samulski, J. Mater. Chem. 11 (2001) 2901.
[14] J. Goldberger, R.R. He, Y.F. Zhang, S.K. Lee, H.Q. Yan, H.J. Choi, P.D. Yang, Nature 422 (2003) 599.
[15] C.N.R. Rao, A. Govindaraj, F.L. Deepak, N.A. Gunari, M. Nath, Appl. Phys. Lett. 78 (2001) 1853.
[16] Y.J. Xiong, Y. Xie, J. Yang, R. Zhang, C.Z. Wu, G. Du, J. Mater. Chem. 12 (2002) 3712.
[17] L. Dloczik, R. Engelhardt, K. Ernst, S. Fiechter, I. Sieber, R. Könenkamp, Appl. Phys. Lett. 78 (2001) 3687.
[18] R. Fan, M. Yue, R. Karnik, A. Majumdar, P.D. Yang, Phys. Rev. Lett. 95 (2005) 0866071.
[19] Y.B. Li, Y. Bando, D. Golberg, Adv. Mater. 16 (2004) 37.
[20] H. Ogihara, S. Takenaka, I. Yamanaka, E. Tanabe, A. Genseki, K. Otsuka, Chem. Mater. 18 (2006) 996.
[21] S. Naito, M. Ue, S. Sakai, T. Miyao, Chem. Commun. (2005) 1563.
[22] R. Riehn, R.H. Austin, J.C. Sturm, Nano Lett. 6 (2006) 1973.
[23] M.C. Chao, H.P. Lin, C.Y. Mou, B.W. Cheng, C.F. Cheng, Catal. Today 97 (2004) 81.
[24] C. Li, Z.T. Liu, C. Gu, X. Xu, Y. Yang, Adv. Mater. 18 (2006) 228.
[25] Y.B. Li, Y. Bando, D. Golberg, Y. Uemura, Appl. Phys. Lett. 83 (2003) 3999.
[26] M. Afzaal, P. O'Brien, J. Mater. Chem. 16 (2006) 1113.
[27] Z.W. Pan, Z.R. Dai, C. Ma, Z.L. Wang, J. Am. Chem. Soc. 124 (2002) 1817.
[28] S.H. Sun, G.W. Meng, M.G. Zhang, Y.F. Hao, X.R. Zhang, L.D. Zhang, J. Phys. Chem. B107 (2003) 13029.
[29] P. Jaffrennou et al., Chem. Phys. Lett. 442 (2007) 372.
[30] P.A. Hu, Y.Q. Liu, L. Fu, L.C. Cao, D.B. Zhu, Appl. Phys. A 80 (2005) 1413.
[31] V.I. Gerasimova et al., Quant. Electro. 33 (2003) 90.
[32] T.B. Massalski, H. Okamoto, P.R. Subramanian, L. Kacprozak, Binary Alloy Phase Diagrams, second edn., ASM International, Materials Park, OH, 1992.
[33] F.H. Lu, H.Y. Chen, Thin Solid Films 355 (1999) 374.
[34] D.R. Lide, Chemical Rubber Company Handbook of Chemistry and Physics, 78th edn., CRC Press, Boca Raton, New York, 1997–1998.
[35] Y.A. Guloyan, Glass Ceram. 61 (2004) 357.